Correction published 9 December 2006

Evaluation of the simulation of the annual cycle of Arctic and Antarctic sea ice coverages by 11 major global climate models

Claire L. Parkinson,[1] Konstantin Y. Vinnikov,[2] and Donald J. Cavalieri[1]

Received 21 November 2005; revised 26 March 2006; accepted 13 April 2006; published 14 July 2006.

[1] Comparison of polar sea ice results from 11 major global climate models (GCMs) and satellite-derived observations for 1979–2004 reveals that each of the models is simulating annual cycles that are phased at least approximately correctly in both hemispheres. Each is also simulating various key aspects of the observed ice cover distributions, such as winter ice not only throughout the central Arctic basin but also throughout Hudson Bay, despite its relatively low latitudes. However, some of the models simulate too much ice, others simulate too little ice (in some cases depending on hemisphere and/or season), and some match the observations better in one season versus another. Several models do noticeably better in the Northern Hemisphere than in the Southern Hemisphere, and one does noticeably better in the Southern Hemisphere. In the Northern Hemisphere all simulate monthly average ice extents to within $\pm 5.1 \times 10^6$ km^2 of the observed ice extent throughout the year; in the Southern Hemisphere all except one simulate the monthly averages to within $\pm 6.3 \times 10^6$ km^2 of the observed values. All the models properly simulate a lack of winter ice to the west of Norway; however, most obtain more ice immediately north of Norway than the observations show, suggesting an under simulation of the North Atlantic Current. The spread in monthly averaged ice extents among the 11 model simulations is greater in the Southern Hemisphere than in the Northern Hemisphere and greatest in the Southern Hemisphere winter and spring.

Citation: Parkinson, C. L., K. Y. Vinnikov, and D. J. Cavalieri (2006), Evaluation of the simulation of the annual cycle of Arctic and Antarctic sea ice coverages by 11 major global climate models, *J. Geophys. Res.*, *111*, C07012, doi:10.1029/2005JC003408.

1. Introduction

[2] Considerable attention has been drawn to the difficulties that models have in simulating the polar regions [e.g., *Serreze et al.*, 2000; *Proshutinsky et al.*, 2001; *Walsh et al.*, 2002]. In addition to numerical complications when the pole is treated as a singularity, these regions (Figure 1) also have the complication of having a variable, ever-changing sea ice cover spreading over much of the ocean area. This ice cover restricts exchanges of heat, mass, and momentum between the ocean and atmosphere, strongly reflects incoming solar radiation, provides a net transport of relatively fresh and cold water equatorward, and affects the salinity and density structure of the underlying ocean [e.g., *Gordon and Taylor*, 1975; *Aagaard and Carmack*, 1989; *Barry et al.*, 1993; *Parkinson*, 2004]. Because of the strong coupling between sea ice and the rest of the climate system, errors in the simulation of the sea ice cover will be propagated to errors in the simulated atmosphere and ocean as well.

[3] In this paper we examine how well 11 major global climate models (GCMs) are simulating the current sea ice covers of the two hemispheres, using as our comparative data set the observed sea ice coverages derived from satellite passive-microwave data. Specifically, we examine (1) the spatial distributions of the sea ice covers in March and September and (2) the monthly average sea ice extents throughout the annual cycle, in each case averaging for the 26-year period 1979–2004. The aim of the paper is to show how well the models are doing, including strengths and weaknesses, not to detail the underlying causes of the model differences.

2. Data and Methodology

[4] Simulation results were obtained from the following web site of the Intergovernmental Panel on Climate Change (IPCC): https://esg.llnl.gov:8443/home/publicHomePage.do. These results have been provided by the respective modeling groups for the ongoing evaluations for the IPCC Fourth Assessment Report, updating the earlier IPCC Third Assessment Report [*Houghton et al.*, 2001]. We selected all models with available output files for both sea ice concentration and sea ice thickness, although use only one run,

[1]Cryospheric Sciences Branch, NASA Goddard Space Flight Center, Greenbelt, Maryland, USA.
[2]Department of Meteorology, University of Maryland, College Park, Maryland, USA.

Copyright 2006 by the American Geophysical Union.
0148-0227/06/2005JC003408

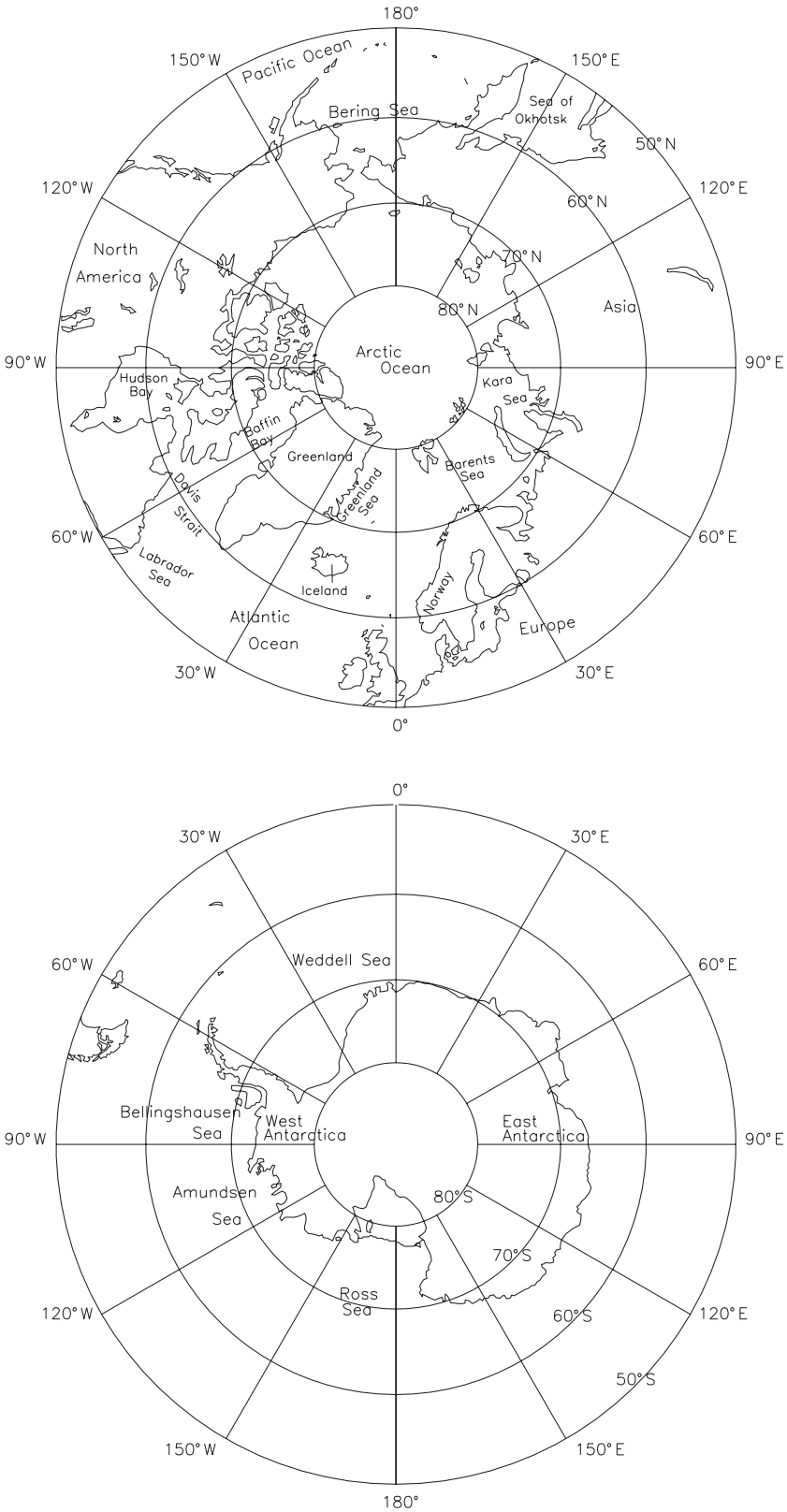

Figure 1. Location maps for the north and south polar regions.

"run1," for each of the models. These models are listed and briefly described in section 3. In each case we use the twentieth century simulation (20C3M) run 1 for the years 1979 through the end of the 20C3M run 1 (i.e., through 1999 or 2000, depending on the model) and its continuation, run 1 of "future climate simulations: scenario SRES A2", for the remaining years through 2004. Each of the 11 models incorporates greenhouse gases and the direct effects of sulfate aerosols in its twentieth century forcings. Some of the models also include additional forcings, as enumerated by *Santer et al.* [2005].

[5] The observational data used to compare with the model results come from the data of the Scanning Multichannel Microwave Radiometer (SMMR) on the Nimbus 7 satellite and the Special Sensor Microwave Imagers (SSMIs) on the Defense Meteorological Satellite Program (DMSP) F8, F11, and F13 satellites. Details on the satellite data sets, their coregistration, and their use in Arctic and Antarctic sea ice studies can be found in the work of *Cavalieri et al.* [1999], *Parkinson et al.* [1999], and *Zwally et al.* [2002]. The SMMR data were collected on an every other day basis for most of the period November 1978 to August 1987, and the SSMI data have been collected on a daily basis for most of the period since the June 1987 launch of the first SSMI, on the DMSP F8. In this paper, we use the SMMR data for January 1979 to August 1987 and the SSMI data for August 1987 to December 2004.

[6] As in the work of *Parkinson et al.* [1999], *Zwally et al.* [2002], and others, ice extent is calculated from the satellite data as the sum of the areas of all grid cells having an ice concentration (percent areal coverage of ice) of at least 15%. For the models, we use the criteria that the ice concentration must be at least 15% and the ice thickness must be at least 6 cm, as the satellite instrument does not sense the extremely thin ice. The 26-year average ice extent, for each month, is calculated by averaging the 26 individual-year ice extents determined for that month. In addition to ice extents, our results (section 4) include maps of the average March and September ice distributions over the 26-year period. Using the 15% ice concentration and 6 cm ice thickness criteria in the individual years, for both March and September averages, we map a pixel as containing ice in the 26-year average March (or September) if and only if that pixel contains ice in at least half the Marches (or Septembers).

3. The Models

[7] The 11 GCMs employed in this study and their IPCC identifications (IDs) are as follows:

[8] 1. The United Kingdom Met Office (UKMO) Hadley Centre Coupled Model 3 (HadCM3) from the Hadley Centre for Climate Prediction and Research at the UKMO, United Kingdom, is a coupled atmosphere-ocean GCM with 19 vertical layers and a horizontal resolution of 2.5° latitude × 3.75° longitude in the atmosphere and 20 vertical layers and a horizontal resolution of 1.25° latitude × 1.25° longitude in the ocean. The sea ice formulation includes ice thermodynamic calculations, one ice layer in the vertical, and ice advection strictly with the ocean current. The ice calculations are divided between the atmosphere and ocean model components. The model shows little drift in surface climate in a control run of over a thousand years, despite not using flux adjustments. The model is described by *Gordon et al.* [2000] and *Pope et al.* [2000]. IPCC ID: UKMO-HadCM3.

[9] 2. The United Kingdom Met Office (UKMO) Hadley Centre Global Environmental Model version 1 (HadGEM1) from the Hadley Centre for Climate Prediction and Research at the UKMO, United Kingdom, is a new coupled climate model developed at the Hadley Centre starting in 2000 as an eventual replacement for the HadCM3 model, with advances in particular in the sea ice and atmosphere components. It has 38 vertical layers and a horizontal resolution of 1.25° latitude × 1.875° longitude in the atmosphere, while in the ocean it has 40 vertical layers, a zonal resolution of 1°, and a meridional resolution that is 1° poleward of 30° and smoothly varies from 0.333° at the equator to 1° at 30° latitude. The sea ice formulation includes ice thermodynamics, ice dynamics, one ice layer in the vertical, and multiple ice thicknesses allowed in a grid cell. The sea ice calculations in the HadGEM1 model, like those in the HadCM3 model, are divided between the atmosphere and ocean components. The HadGEM1 model is described by *Johns et al.* [2005]. IPCC ID: UKMO-HadGEM1.

[10] 3. The European Centre for Medium-Range Weather Forecasts (ECMWF) Hamburg Model version 5 (ECHAM5) from the Max Planck Institute for Meteorology (MPI), Hamburg, Germany, is a fifth-generation ECHAM model using a spectral, semi-implicit formulation for the atmosphere, with 31 vertical layers, and an ocean with 40 vertical layers and 1.5° latitude × 1.5° longitude horizontal resolution. The sea ice formulation includes ice dynamics, ice thermodynamics, one ice layer in the vertical plus an overlying snow layer, one ice thickness category, and 1.5° latitude × 1.5° longitude horizontal resolution. The sea ice calculations are done within the ocean component. The atmosphere component is described by *Roeckner et al.* [2003], and the ocean component is described by *Marsland et al.* [2003]. IPCC ID: ECHAM5/MPI-OM.

[11] 4. The Canadian Centre for Climate Modelling and Analysis (CCCma) Third Generation Coupled Global Climate Model (CGCM3) from the CCCma, Environment Canada, University of Victoria, Canada, is a third-generation model that has a substantially updated atmosphere component over the second-generation CGCM2, with details available at http://www.cccma.bc.ec.gc.ca/models/cgcm3.shtml. Results from two versions of the model, T47 and T63, were provided to the IPCC. We use the results from the lower-resolution T47 version, with 31 vertical layers and a spatial resolution of approximately 3.75° latitude × 3.75° longitude in the atmosphere and 29 vertical layers and a spatial resolution of approximately 1.85° latitude × 1.85° longitude in the ocean. The sea ice formulation includes ice thermodynamics, ice dynamics, and a single ice thickness per grid cell. Details on the model's ocean component can be found in the work of *Kim et al.* [2002]. IPCC ID: CGCM3.1.

[12] 5. The Commonwealth Scientific and Industrial Research Organization (CSIRO) Mark 3.0 model (CSIRO Mk3) from CSIRO, Australia, is a vintage 2001 model with 18 vertical layers and a horizontal resolution of approximately 1.875° latitude × 1.875° longitude in the atmosphere/land/ice component and 31 vertical layers and a

horizontal resolution of approximately 0.84° latitude × 1.875° longitude in the ocean component. The sea ice formulation includes ice thermodynamics, ice dynamics, one or two ice layers in the vertical depending on ice thickness, and an overlying snow layer. The sea ice calculations are done as part of the atmosphere component, with the same spatial resolution. The CSIRO Mark 3.0 model is described in detail by *Gordon et al.* [2002]. IPCC ID: CSIRO-Mk3.0.

[13] 6. The medium resolution version 3.2 of the Model for Interdisciplinary Research on Climate (MIROC3) from the Center for Climate System Research (CCSR) at the University of Tokyo, the Japan National Institute for Environmental Studies (NIES), and the Frontier Research Center for Global Change (FRCGC), Japan, has an atmosphere component with 20 vertical layers and a horizontal resolution approximately equivalent to 2.8° latitude × 2.8° longitude. The ocean component has 43 vertical layers, a zonal resolution of approximately 1.4°, and a meridional resolution varying from approximately 0.56° at low latitudes to approximately 1.4° at high latitudes. The sea ice formulation includes ice thermodynamics, ice dynamics, one ice layer in the vertical and an overlying snow layer, two ice thickness categories allowed in a grid cell, and a spatial resolution of 1.4° in both latitude and longitude. The MIROC model is described by *Hasumi and Emori* [2004]. IPCC ID: MIROC3.2 (medres).

[14] 7. The Bjerknes Centre for Climate Research (BCCR) Bergen Climate Model (BCM) version 2 (BCCR BCM2) from the BCCR at the University of Bergen, Norway, has an atmosphere component with 31 vertical layers and a linear reduced Gaussian grid [*Hortal and Simmonds*, 1991] equivalent to approximately 2.8° latitude × 2.8° longitude spatial resolution. The ocean component has 35 vertical layers, 1.5° zonal resolution, and meridional resolution varying from 0.5° to 1.5° depending on latitude. The sea ice formulation includes ice thermodynamics, ice dynamics, one ice layer in the vertical overlain by a snow layer, and a single ice thickness per grid cell. The ice calculations are done within the model's ocean component, with four ice grid cells within each ocean grid cell. Additional information can be found in the work of *Furevik et al.* [2003] and at http://www-pcmdi.llnl.gov/ipcc/model_documentation/BCCR_BCM2.0.pdf. IPCC ID: BCCR-BCM2.0.

[15] 8. The Goddard Institute for Space Studies (GISS) model ER (GISS ER) from GISS, National Aeronautics and Space Administration (NASA), United States, incorporates the GISS Model E atmospheric GCM, described in detail by *Schmidt et al.* [2006]. "E" here has no meaning beyond being the next letter in the alphabet in a list of GISS models. "R" refers to the coupling of Model E with an ocean model whose development was led by G. Russell. Model ER has 20 vertical layers in the atmosphere, 13 vertical layers in the ocean, and a spatial resolution of 4° latitude × 5° longitude for both the atmosphere and ocean components. The sea ice formulation includes ice thermodynamics, ice dynamics, four ice layers in the vertical overlain by one snow layer, and one ice thickness category per grid cell. The ice calculations are incorporated as part of the model's atmosphere component, with the same resolution. Additional information can be found in the work of *Schmidt et al.* [2006] and *Russell et al.* [2000]. IPCC ID: GISS ER.

[16] 9. The Institut Pierre Simon Laplace (IPSL) coupled model 4 (IPSL CM4) from IPSL, France, has an atmosphere component with 19 vertical layers and a spatial resolution of 2.5° latitude × 3.75° longitude. It is described by F. Hourdin et al. (The LMDZ4 general circulation model: Climate performance and sensitivity to parameterized physics with emphasis on tropical convection, submitted to *Climate Dynamics*, 2005, hereinafter referred to as submitted manuscript, 2005). The ocean component has 31 vertical layers, a spatial resolution of 2° latitude × 2° longitude, and a tripolar grid, with one pole at the South Pole, one over Canada, and one over Siberia, avoiding a singularity at the North Pole. The sea ice formulation includes ice thermodynamics, ice dynamics, two ice layers in the vertical overlain by a snow layer, and a spatial resolution as in the ocean model, 2° latitude × 2° longitude. Further details can be found in the work of *Marti et al.* [2005]. IPCC ID: IPSL-CM4.

[17] 10. The Institute of Numerical Mathematics (INM) CM3.0 model (INM CM3) from INM, Russian Academy of Sciences, Russia, has an atmosphere component with 21 vertical layers and a spatial resolution of 4° latitude × 5° longitude. The ocean component has 33 vertical layers, a rigid lid, and a spatial resolution of 2° latitude × 2.5° longitude. Both the atmosphere and ocean components have sigma vertical coordinates. The sea ice formulation is strictly thermodynamic, with one layer in the vertical, one thickness category, and the same spatial resolution as for the ocean component. Further details can be found in the work of *Diansky et al.* [2002] and *Diansky and Volodin* [2002]. IPCC ID: INM-CM3.0.

[18] 11. The Geophysical Fluid Dynamics Laboratory (GFDL) coupled model 2.1 (GFDL CM2.1) from GFDL, National Oceanic and Atmospheric Administration (NOAA), United States, has an atmosphere component with 24 vertical layers and a horizontal resolution of 2° latitude × 2.5° longitude, with a hybrid sigma-pressure vertical coordinate. The ocean component has 50 vertical layers and 1° latitude × 1° longitude horizontal resolution at middle and high latitudes, with enhanced resolution in the tropics, down to 0.333° at the equator, and with poles over North America and Eurasia to avoid complications at the geographic North Pole. The sea ice formulation includes ice thermodynamics, ice dynamics, two ice layers overlain by one snow layer, five thickness categories allowed in a grid cell, and the same horizontal grid as used in the ocean component. The CM2.1 model does not employ flux adjustments. Additional details about the GFDL CM2.1 model can be found in the work of *Zhang and Delworth* [2005] and *Delworth et al.* [2006]. IPCC ID: GFDL-CM2.1.

[19] Table 1 provides a compact summary of the model names, the horizontal resolutions and number of vertical layers in both the atmosphere and ocean components, and sources for additional information.

4. Results

[20] Figure 2 presents summer and winter sea ice distributions from the satellite observations (Figure 2a) and from each of the 11 models (Figures 2b–2l), averaged over the 26

Table 1. Model Summary for the 11 Models Used in the Analysis[a]

Model	Atmosphere Component	Ocean Component	References
HadCM3, United Kingdom	19 vertical layers; 2.5° lat. × 3.75° long.	20 vertical layers; 1.25° lat. × 1.25° long.	*Gordon et al.* [2000], *Pope et al.* [2000]
HadGEM1, United Kingdom	38 vertical layers; 1.25° lat. × 1.875° long.	40 vertical layers; 1° lat. × 0.333–1° long.	*Johns et al.* [2005]
ECHAM5, Germany	31 vertical layers; spectral, semi-implicit	40 vertical layers; 1.5° lat. × 1.5° long.	*Roeckner et al.* [2003], *Marsland et al.* [2003]
CGCM3, Canada	31 vertical layers; ~3.75° lat. × 3.75° long.	29 vertical layers; ~1.85° lat. × 1.85° long.	*Kim et al.* [2002]
CSIRO Mk3, Australia	18 vertical layers; ~1.875° lat. × 1.875° long.	31 vertical layers; ~0.84° lat. × 1.875° long.	*Gordon et al.* [2002]
MIROC3, Japan	20 vertical layers; ~2.8° lat. × 2.8° long.	43 vertical layers; ~1.4° lat. × 0.56–1.4° long.	*Hasumi and Emori* [2004]
BCCR BCM2, Norway	31 vertical layers; ~2.8° lat. × 2.8° long.	35 vertical layers; 1.5° lat. × 0.5–1.5° long.	*Furevik et al.* [2003]
GISS ER, United States	20 vertical layers; 4° lat. × 5° long.	13 vertical layers; 4° lat. × 5° long.	*Schmidt et al.* [2006], *Russell et al.* [2000]
IPSL CM4, France	19 vertical layers; 2.5° lat. × 3.75° long.	31 vertical layers; 2° lat. × 2° long.	F. Hourdin et al. (submitted manuscript 2005), *Marti et al.* [2005]
INM CM3, Russia	21 vertical layers; 4° lat. × 5° long.	33 vertical layers; 2° lat. × 2.5° long.	*Diansky et al.* [2002], *Diansky and Volodin* [2002]
GFDL CM2.1, United States	24 vertical layers; 2° lat. × 2.5° long.	50 vertical layers; 0.333–1° lat. × 0.333–1° long.	*Zhang and Delworth* [2005], *Delworth et al.* [2006]

[a]See section 3 for information on the sea ice calculations, which are incorporated in the atmosphere component in some cases and in the ocean component in other cases.

years 1979–2004. Results are presented for September and March of each hemisphere. In the Northern Hemisphere, September is typically the month of minimum ice coverage and March is typically the month of maximum ice coverage. In the Southern Hemisphere, September is often the month of maximum ice coverage, although maximum ice coverage can alternatively occur in either August or October. February is generally the month of minimum ice coverage in the Southern Hemisphere, with the ice cover growing somewhat in March, at the end of summer and start of autumn.

[21] Figure 3 presents the full annual cycle of monthly average ice extents for both hemispheres, again averaged for 1979–2004, first from the observations (Figure 3a) and then from simulations of the 11 GCMs (Figures 3b–3l). The observations show the 26-year-average Arctic sea ice cover reaching a minimum extent of 6.8×10^6 km^2 in September and rising to a maximum extent of 15.3×10^6 km^2 in March and the 26-year-average Antarctic sea ice cover reaching a minimum extent of 3.0×10^6 km^2 in February and rising to a maximum extent of 18.2×10^6 km^2 in September (Figure 3a).

[22] Although each model properly simulates out-of-phase annual cycles in the two hemispheres, with low ice amounts near the end of the respective summers and high ice amounts near the end of the respective winters, the phasing and especially the amplitudes of the cycles vary noticeably among the models, as does the closeness of the match of the simulated ice covers to the observations (Figure 3). The UK HadCM3 model simulates several aspects of the annual cycle of ice extents quite well, although maximum simulated ice extents in both hemispheres are higher than in the observations and are delayed by about a month versus the observations (Figure 3b). The March map shows that the excess Northern Hemisphere winter ice is largely in the Greenland and Barents Seas (Figure 2b), suggesting an under simulation of the Gulf Stream and North Atlantic Current. The Southern Hemisphere HadCM3 map shows too little late winter ice in the vicinity of the Greenwich meridian but too much late winter ice from 70°E eastward to 100°W and too little summertime ice in the Western Hemisphere (Figure 2b).

[23] The UK HadGEM1 model simulates greater ice extents than the observations throughout the year, with the excess versus the observations being particularly large in the Southern Hemisphere winter (Figure 3c). This model simulates the correct timing of minimum ice extent in both hemispheres and of maximum ice extent in the Northern Hemisphere, while simulating maximum Southern Hemisphere ice coverage as occurring in October, one month delayed versus the observations (Figure 3c). The Northern Hemisphere March map shows a very good match with the observed pattern of ice coverage throughout the entire North Atlantic vicinity (Labrador Sea, Davis Strait, Greenland Sea, Barents Sea), although with somewhat too much ice in the Barents Sea. On the Pacific side, there is too much March ice in both the Bering and Okhotsk seas. Summertime ice is too extensive in Baffin Bay and immediately north of western Canada and Alaska, although is somewhat less extensive than the observations in the Greenland Sea and just north of the Barents and Kara seas. HadGEM1

Figure 2. Areal distributions of Northern and Southern Hemisphere March and September sea ice covers, averaged over 1979–2004, (a) as observed from satellite data and (b–l) as simulated by each of 11 major global climate models (GCMs). In each case the late summer sea ice distribution (September in the Northern Hemisphere and March in the Southern Hemisphere) is depicted in dark shading, and the late winter sea ice distribution (March in the Northern Hemisphere and September in the Southern Hemisphere) extends over both the dark and light shaded regions.

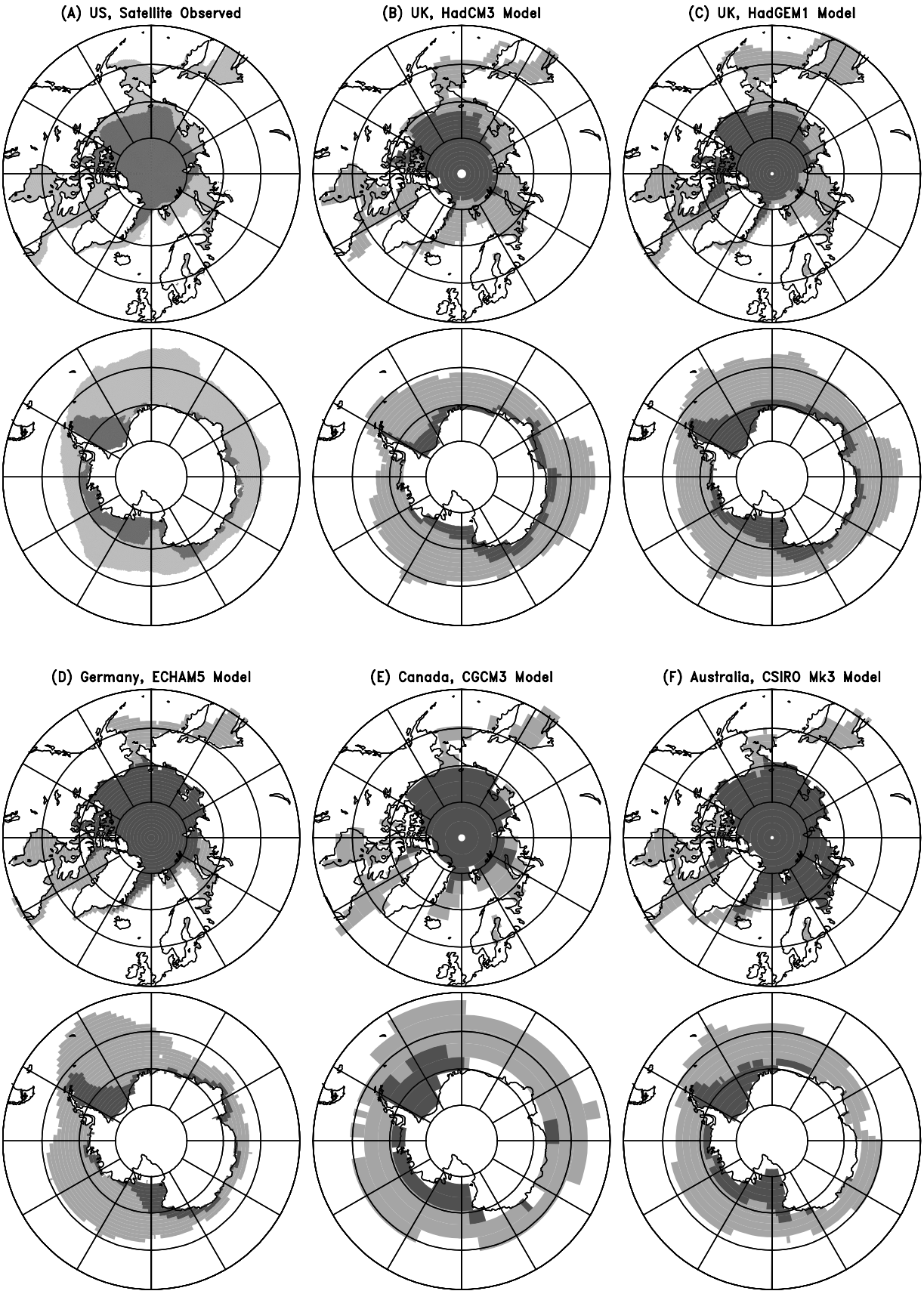
(A) US, Satellite Observed
(B) UK, HadCM3 Model
(C) UK, HadGEM1 Model
(D) Germany, ECHAM5 Model
(E) Canada, CGCM3 Model
(F) Australia, CSIRO Mk3 Model

Figure 2

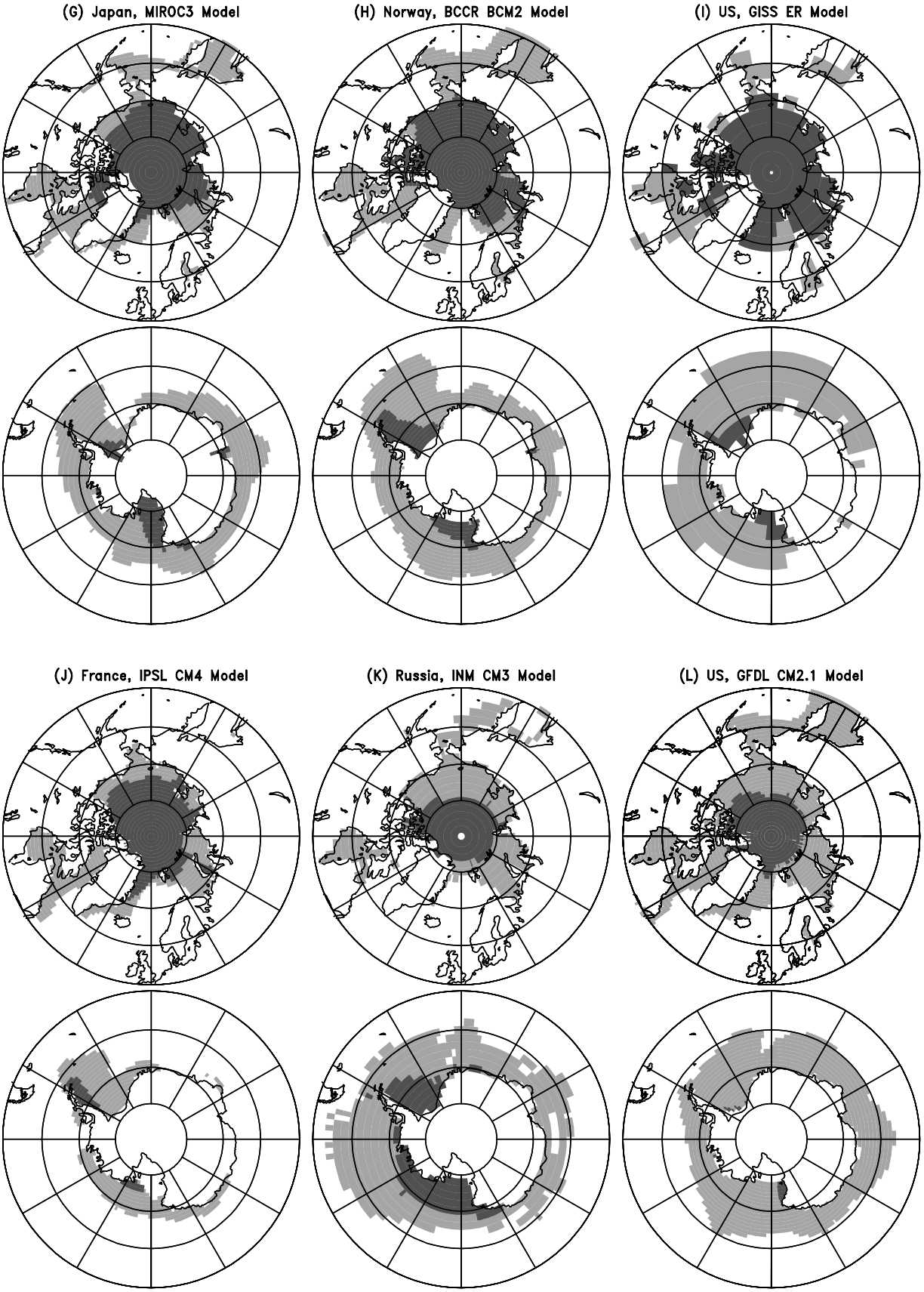

Figure 2. (continued)

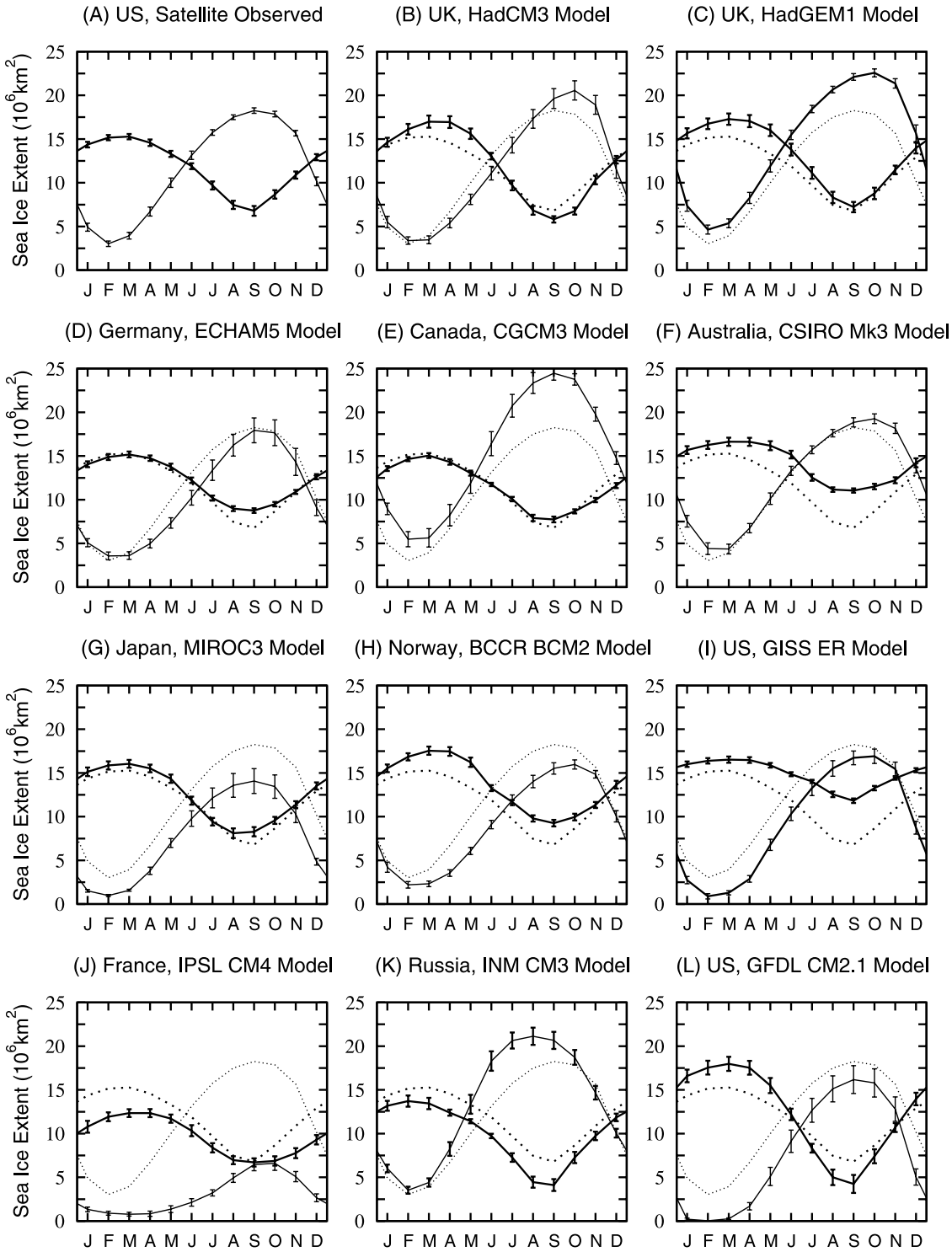

Figure 3. Annual cycle of monthly sea ice extents, averaged over 1979–2004, (a) as observed from satellite data and (b–l) as simulated by each of 11 major GCMs, for the Northern (thickest curves) and Southern (thinner curves) Hemispheres. The observed results from Figure 3a are repeated on each of the other plots, as dotted curves, for comparison purposes. Vertical bars show the standard deviations of the monthly mean ice extents.

successfully simulates more Northern Hemisphere summer ice than HadCM3 (Figure 2c versus 2b). In the Southern Hemisphere, the geographic pattern of the wintertime ice cover simulated by HadGEM1 is improved over that of HadCM3, although the ice cover is excessive around much of the continent. The simulation of the pattern of summertime ice has also improved, especially in the western Weddell Sea, although the ice amount is excessive, with

the excess ice coming largely in the eastern Weddell Sea and the Eastern Hemisphere (Figure 2c).

[24] The German ECHAM5 model properly simulates the timing of maximum and minimum ice coverage in both hemispheres and for all except the summer months, even simulates the correct magnitudes of the ice extents in the Northern Hemisphere. The simulated extent magnitudes are also close to the observed values in the Southern Hemisphere throughout the decay period, while being too low during the growth period (Figure 3d). The distribution of simulated March ice cover in the Northern Hemisphere is excellent, while the simulated September ice is somewhat too great around the entire periphery of the ice cover, inappropriately spreading southward to the western Canadian, Alaskan, and Russian coasts, as well as being excessive in the Greenland Sea and the northern Barents and Kara Seas (Figure 2d), although the entire excess is less than 30% (Figure 3d). In the Southern Hemisphere, the simulated September, late-winter ice is too extensive in the western Weddell Sea, especially near 30°W, and in the Amundsen Sea, but is not extensive enough in the eastern Weddell Sea and around much of East Antarctica (Figure 2d). The excesses and underestimates balance each other so well that the ice extent for September is within 2% of the observed extent (Figure 3d). The simulated March Southern Hemisphere ice distributions are reasonable around much of the continent although with too little ice in the Amundsen and eastern Ross Seas and too much ice in the western Ross Sea (Figure 2d).

[25] The Canadian CGCM3 model simulates correct maximum and minimum timings in both hemispheres and does an excellent job in simulating the annual cycle of Northern Hemisphere ice extent magnitudes although simulates considerably too much Southern Hemisphere ice, especially in winter (Figure 3e). Spatially, the coarse resolution of the T47 model grid prohibits a simulation of the details of the ice edge, but to the level allowed by the resolution, the model does very well in simulating the winter ice in the Sea of Okhotsk and Hudson Bay and the absence of ice west of Norway. Excessive ice coverage appears in the Labrador Sea and immediately north of Iceland and Finland, while too little ice appears along the southeast coast of Greenland. In September, somewhat excessive ice coverage appears around most of the periphery of the central Arctic Basin and too little ice appears to the east of Greenland, although in many areas the differences from the observations can be accounted for by the coarse model resolution. In the Southern Hemisphere, excess wintertime ice appears around most of the continent and excess summertime ice appears especially in the eastern Weddell Sea (Figure 2e).

[26] In contrast to the Canadian CGCM3 model, with its superior simulation of the Northern Hemisphere ice cover, the Australian CSIRO Mk3 model does a superior job in the simulation of the Southern Hemisphere ice. The CSIRO Mk3 Southern Hemisphere simulation has ice extents matching the observed values almost precisely for much of the growth period, although has a month delay in the timing of minimum and maximum ice coverage and somewhat too much ice in the ice decay period. The Northern Hemisphere simulation has too much ice throughout the year but especially in summer, with a resulting under simulation of the amplitude of the annual cycle (Figure 3f). Spatially, the significant excess of ice in the Northern Hemisphere summer appears most prominently in the Kara and Barents Seas, although is also apparent in the existence of ice in northern Baffin Bay and the extension of the central Arctic ice to the North American, Asian, and European coasts. The excessive ice in both summer and winter seasons in the Barents Sea suggests an under simulation of the Gulf Stream and North Atlantic Current. Wintertime ice in the Greenland Sea is also excessive, while that in the Bering Sea is underrepresented (Figure 2f). Simulation of the Southern Hemisphere ice distributions is considerably better, although with too much late-summer ice in the western Ross and eastern Weddell Seas and too little summer ice around much of East Antarctica (Figure 2f).

[27] Like the Canadian model, the Japanese MIROC3 model does a far better job in simulating the Northern Hemisphere ice than the Southern Hemisphere ice. The MIROC3 results in the Southern Hemisphere have the timing of maximum and minimum ice extent correct and a quite reasonable amplitude for the annual cycle but have too little ice throughout the year (Figure 3g). The MIROC3 Northern Hemisphere ice extents are much closer in magnitude to the observations, with the difference between simulated and observed monthly average extents being greatest in September, and even then the excess in simulated ice extent is only 22%. This excess is due in part to the early simulated ending of the decay period, minimum ice extent coming in August rather than September (Figure 3g). Spatially, the Southern Hemisphere September modeled results have too little ice in the Amundsen, eastern Ross, and especially the eastern Weddell Sea, with an interesting capturing of a pattern of ice in the western Weddell Sea reflective of the clockwise Weddell Gyre that is sometimes seen in the observations, although in the December–May time frame rather than in September. The Southern Hemisphere March simulation results have too little ice in the western Weddell Sea and in the southern Bellingshausen and Amundsen Seas and eastern Ross Sea, with too much ice in the western Ross Sea (Figure 2g). In the Northern Hemisphere, the excess Northern Hemisphere summer ice simulated by the model is predominantly immediately north of Eurasia and in northern Baffin Bay, whereas most of the small amount of excess wintertime ice is in the Barents Sea and eastern Sea of Okhotsk, suggestive of a weak North Atlantic Current and a weak eastern Okhotsk current (Figure 2g).

[28] The Norwegian BCCR BCM2 model simulates annual cycles with amplitudes matching well with the observations in both hemispheres. There is, however, too little ice simulated in the Antarctic and too much ice in the Arctic, with the timing of minimum monthly average ice extent correct in both cases but the timing of maximum ice extent delayed by one month in the Southern Hemisphere (Figure 3h). Spatially, the excess Northern Hemisphere wintertime ice is apparent in the Bering Sea, Sea of Okhotsk, Barents Sea, and north of Iceland, with too little ice simulated in the Labrador Sea and along the southeastern coast of Greenland. In late summer, most of the excess ice is in the Kara and Barents Seas and immediately north of Russia. In the Southern Hemisphere, the region most

deficient in simulated September (winter) ice is the eastern Weddell Sea and the region most deficient in simulated March (summer) ice is the Amundsen and eastern Ross Seas. In contrast, the western Ross Sea contains a slight excess of simulated summer ice and the Weddell Sea has a realistic simulated summer ice cover, with substantial ice in the western portion of the sea and no ice in the eastern portion (Figure 2h).

[29] The U.S. GISS ER model does a good job at simulating the amplitude of the annual cycle in the Southern Hemisphere, although with too little ice through much of the year and a 1-month delay, until October, in the reaching of maximum ice coverage. In the Northern Hemisphere, too much ice is simulated throughout the year, especially in summer, with the result that the amplitude of the annual cycle is under simulated (Figure 3i). The coarse resolution of the model grid is apparent in the maps and hinders simulation of the details of the ice edge. In both the March and September Northern Hemisphere results, the excess ice is particularly apparent in the Barents Sea and the northern Greenland Sea. The simulation of ice throughout the Barents Sea even in summertime suggests a strong under simulation of the northward water flow from the North Atlantic Current. The under simulation of Southern Hemisphere ice is apparent in the lack of ice along most of the East Antarctic coast from about 75°E to about 160°E in both March and September, likely in part (although not entirely) because of the coarse model resolution. In March there is also a notable absence of ice in the Bellingshausen and Amundsen Seas and too little ice in the western Weddell Sea. In wintertime, there is too much ice in the Amundsen Sea but appropriate ice distributions, to the resolution of the model, in the Weddell Sea and east to about 75°E and in much of the Ross and Bellingshausen Seas (Figure 2i).

[30] The French IPSL CM4 model does a much better job at simulating the Northern than the Southern Hemisphere ice cover, although fails to simulate enough ice in either hemisphere. The Southern Hemisphere simulation in particular has considerably too little ice, with the ice throughout the year being less than 37% of the observed values and in all months except September and October being less than 30% of the observed values (Figure 3j). Furthermore, the timings of minimum and maximum ice coverage are both about one month late. Spatially, the September Southern Hemisphere winter ice cover is appropriate in the western Weddell Sea and off East Antarctica at about 140°E but not extensive enough around the rest of the continent. The simulated March ice cover is well under the observed amounts but does properly show that the greatest amount of late summer ice is in the western Weddell Sea. In contrast, the Northern Hemisphere simulated ice distributions are much closer to the observations, especially in September, when the simulated distribution is excellent, having an appropriately positioned tongue of ice along the east coast of Greenland, an appropriate simulation of ice along the north coast of Greenland and the northernmost Canadian islands, and an appropriate retreat of the ice from the Alaskan and much of the Russian coast. The simulated Northern Hemisphere March ice cover has too little ice in the Bering and Okhotsk Seas but an appropriate ice distribution in Davis Strait and the Labrador Sea. The IPSL CM4 model does much better than many models in simulating the warming influence of the North Atlantic Current as far north as north of Norway and the extension of the tongue of ice along the east coast of Greenland almost to the southern tip of the island. Although there is somewhat too much ice in this North Atlantic region, overall the pattern of wintertime ice distributions in this region is excellent (Figure 2j).

[31] The Russian INM CM3 model does well in simulating the amplitude of the Northern Hemisphere annual cycle and the timing of minimum ice extent, although with too little ice in each month. In the Southern Hemisphere it does well in simulating ice extents in spring and summer but simulates too great and rapid an expansion of the ice cover in autumn and early winter, with a peak ice extent of 21×10^6 km^2 in August, a month prior to the observed monthly average peak of 18.2×10^6 km^2 in September (Figure 3k). Spatially, there is a proper simulation of the March wintertime ice covering the Arctic Basin, the Kara Sea, and Hudson Bay, but too little winter ice in Baffin Bay, the Labrador Sea, along the east coast of Greenland and in the Sea of Okhotsk, canceled in part by too much winter ice in the Barents Sea and western Bering Sea. Simulated September Northern Hemisphere ice is properly centered slightly to the Bering Strait side of the North Pole but is not as extensive as the observed ice cover. In the Southern Hemisphere, the pattern of March late-summer ice is simulated quite well, although with too much ice in the Ross Sea. The simulated pattern of Southern Hemisphere September late-winter ice has considerably too extensive an ice cover in the Bellingshausen and Amundsen Seas and too little ice in the eastern Weddell Sea (Figure 2k).

[32] The U.S. GFDL CM2.1 model simulates the amplitude of the annual cycle in the Southern Hemisphere quite well, although with too little ice throughout the year. It also properly simulates the timing of maximum and minimum ice extents in both hemispheres. In the Northern Hemisphere, the GFDL simulation obtains too much ice in the winter and too little ice in the summer, resulting in an amplified annual cycle (Figure 3l). The GFDL results have the Southern Hemisphere ice cover reduced to only 0.03×10^6 km^2 in February (versus the observed 3.03×10^6 km^2) (Figure 3l), with a small amount of ice beginning to form at coastal locations in March (Figure 2l), well under the observed March ice coverage (Figure 2a). The September distribution of the Southern Hemisphere ice is excellent around most of the Antarctic continent except in the Weddell Sea, where there is too little ice (Figure 2l). The Northern Hemisphere March simulated ice distribution shows the excess wintertime ice to be most apparent on the Pacific side, in the Bering Sea and Sea of Okhotsk, with some excess ice also in the eastern Barents Sea and the Greenland Sea. The wintertime ice distributions in the Davis Strait and Labrador Sea regions are excellent. The simulated Northern Hemisphere summertime ice is not nearly extensive enough but otherwise is well distributed (Figure 2l).

[33] All 11 models properly simulate that Hudson Bay, despite its low latitudes, is covered with ice in March, and all except one of the models properly simulate that this ice has totally retreated from the bay in September (Figure 2). They also all properly simulate that there is no ice from the west of Norway to the Greenwich meridian along most of the Norwegian coast even in March and that wintertime ice fully covers the Arctic Basin (to at least 15% ice coverage in

each grid cell). In the Southern Hemisphere, 9 of the 11 models properly simulate that wintertime ice completely surrounds the continent of Antarctica and most also properly simulate that summertime sea ice is predominantly in the Western Hemisphere, due largely to the greater northward extension of the continent in the Eastern Hemisphere (Figure 2).

[34] Figure 3 includes for each monthly average a vertical bar showing the standard deviation of the 26 values for that month over the 1979–2004 period. This provides a measure of the variability of the observations and the model results around their respective mean states. The variability in the observations is similar in the two hemispheres, with the monthly standard deviations ranging from 0.30×10^6 km^2 (in February) to 0.56×10^6 km^2 (in September) in the Northern Hemisphere and from 0.27×10^6 km^2 (in August) to 0.54×10^6 km^2 (in May) in the Southern Hemisphere (Figure 3). This is not the case, however, for the simulated variabilities. For the Northern Hemisphere, half the models simulate standard deviations below 0.6×10^6 km^2 in each month, consistent with the observations, and some of these models simulate standard deviations below the observed values. For the Southern Hemisphere, in contrast, none of the model simulations has all 12 standard deviations below 0.6×10^6 km^2, and many of the models simulate markedly greater variability, with standard deviations ranging up to 1.61×10^6 km^2 in October for the GFDL model. In fact, although the observations tend to have low standard deviations in the Southern Hemisphere during the peak ice months (July–November), over half the models (Hadley CM3, ECHAM5, MIROC3, BCCR BCM2, GISS ER, IPSL CM4, and GFDL CM2.1) have their highest standard deviations in the Southern Hemisphere during these months (Figure 3). This excessive Southern Hemisphere winter/spring sea ice variability in the simulations versus the observations could reflect an excessive modeled variability in the winter/spring Southern Ocean temperatures or polar front. Interestingly, the ECHAM5, CGCM3, and MIROC3 models, all of which have results matching the observations better in the Northern Hemisphere than in the Southern Hemisphere, also have considerably smaller standard deviations in the Northern Hemisphere. In general though, the size of the standard deviations does not have a strong correspondence with how well the simulation matches the observations, as illustrated especially prominently by the small standard deviations in the IPSL CM4 model throughout the Southern Hemisphere annual cycle despite the unrealistically low simulated ice extents. In general, the models that produce too little (or too much) ice in a particular hemisphere and season do so consistently throughout the 1979–2004 period (Figure 3). Presentation and discussion of the sea ice trends simulated by the 11 models for the 1972–2004 period can be found in the work of *Vinnikov et al.* [2006].

5. Summary and Discussion

[35] Sea ice results from 11 major GCM simulations have been compared with satellite observed sea ice extents averaged by month for the period 1979–2004. Each model appropriately simulates an annual cycle with greater ice extent in the winter than the summer of each hemisphere, and each model appropriately simulates certain basic observed features, such as an ice-covered Hudson Bay in winter, despite its relatively low latitudes, and an ice-free span from Iceland to Norway, despite its higher latitudes. However, some models simulate too much ice, others too little ice (in some cases varying depending on hemisphere and/or season), and some models match the observations noticeably better in either the growth or decay season. Similarly, some models match the observations better in the Northern Hemisphere (e.g., the CGCM3 and the MIROC3) and others match the observations better in the Southern Hemisphere (e.g., the CSIRO Mk3).

[36] With all GCMs, attention to individual model components or regions can result in tuning that selectively improves the model results. Likely the superior performance of the German, Canadian, French, and Japanese models in the Northern versus Southern Hemisphere and the superior performance of the Australian model in the Southern versus Northern Hemisphere (Figures 2 and 3) result at least in part from greater attention being paid to the results in their respective hemispheres. Similarly, the much better performance of the French model (and, to a lesser extent, the Norwegian and UK HadGEM1 models) in the Atlantic versus the Pacific portion of the sub-Arctic (Figure 2j and, secondarily, Figures 2c and 2h) could result from a greater interest in the Atlantic region, even if the attention was toward the atmospheric and oceanic circulations, affecting weather conditions in France (or Norway or the UK), rather than specifically toward the sea ice.

[37] By and large, the models do a much better job at simulating the latitudinally asymmetric spatial patterns of the Northern Hemisphere ice than the Southern Hemisphere ice. All 11 models correctly simulate at least some late-winter ice-free water north of 70°N between Greenland and Scandinavia despite the high latitudes while also correctly simulating ice south of 60°N in Hudson Bay and, except for one model, ice also south of 60°N in the Labrador Sea (Figure 2). Yet most of these same models do not simulate the observed pattern whereby the Antarctic wintertime ice extends farthest equatorward at about 0–20°E (Figure 2). This suggests a much better simulation of the ocean circulation in the North Atlantic, and especially the powerful impact of the northeastward flowing Gulf Stream and North Atlantic Current (despite the full impact not being simulated, as identified in section 4), than of the ocean circulation in the Southern Ocean. This is not unexpected, in light of the attention that the Gulf Stream has received historically, owing to its importance both to the climate of Europe and to shipping across the North Atlantic. This attention goes back at least to the eighteenth century, as reflected in the Gulf Stream chart prepared by Benjamin Franklin and Timothy Folger in the 1760s [*Richardson*, 1980], and the Gulf Stream has naturally been a key oceanographic feature for the modeling community to focus on, in the attempt to simulate it accurately. Once greater attention is paid to Southern Hemisphere ocean circulations, the pattern of Southern Hemisphere sea ice distributions can be expected to improve also.

[38] When the annual cycles of the ice extent differences between the simulated and observed results for each of the 11 models are plotted together (Figure 4), it becomes clear that, overall, the modeled annual cycles are more similar

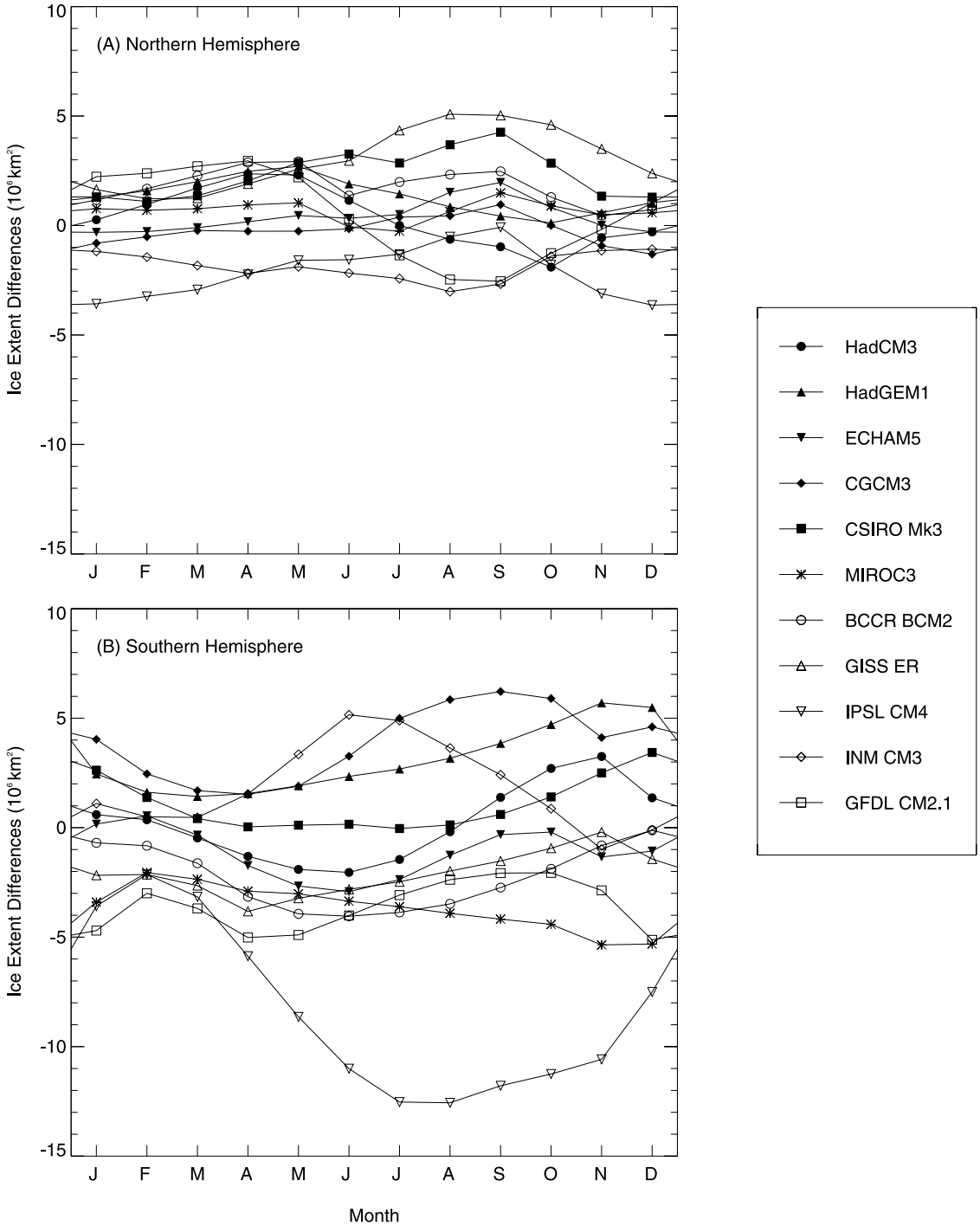

Figure 4. Difference between the modeled 1979–2004 monthly average sea ice extents and the satellite-based observations (modeled minus observed), for each of 11 major GCMs, for both the (a) Northern Hemisphere and (b) Southern Hemisphere.

among themselves and closer to the observations in the Northern Hemisphere than in the Southern Hemisphere, consistent with the greater attention being paid by most modeling groups to the Northern Hemisphere conditions. In the Northern Hemisphere, all monthly average modeled ice extents lie within $\pm 5.1 \times 10^6$ km^2 of the observed ice extent throughout the year, and the spread among the models is greatest in the summer and autumn months, especially August and September (Figure 4a). In the Southern Hemisphere, there is a noticeably larger spread among the model results, although still all models except one have simulated monthly average ice extents that consistently lie within $\pm 6.3 \times 10^6$ km^2 of the observed ice extents (Figure 4b). In contrast to the Northern Hemisphere, in the Southern Hemisphere the greatest spread among the model results occurs during the winter and spring months (Figure 4).

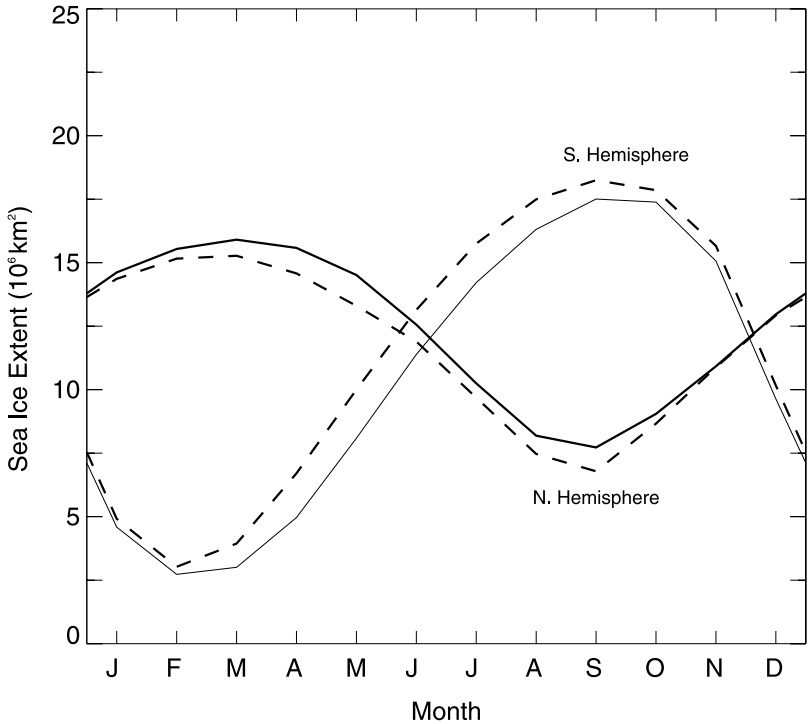

Figure 5. Annual cycle of monthly sea ice extents, averaged over 1979–2004, from satellite data (dashed curves) and from the averaged results from 11 major GCMs (solid curves), for the Northern and Southern Hemispheres.

[39] Despite the variety of problems with the individual simulations, when the results from the 11 models are averaged, the ensemble average of the model simulations does quite well in simulating the annual cycle of sea ice extents in each hemisphere, although with the interesting contrast that the ensemble Northern Hemisphere monthly averages are all greater than the observations while the ensemble Southern Hemisphere monthly averages are all less than the observations (Figure 5). Percentage-wise, the Northern Hemisphere averages exceed the observations by values ranging from 0.3% in December to 13.9% in September and the Southern Hemisphere averages are less than the observations by values ranging from 2.6% in October to 26.0% in April. In terms of monthly ice extents, the Northern Hemisphere ensemble averages are greater than the observed by amounts ranging from 0.04×10^6 km^2 in December to 1.2×10^6 km^2 in May and the Southern Hemisphere averages are less than the observed by amounts ranging from 0.3×10^6 km^2 in February to 1.9×10^6 km^2 in May.

[40] Using the root mean square (RMS) of the 12 monthly departures from the observed ice extents as one measure of how well a model is performing overall, the 11-model composite (with an RMS of 1.2×10^6 km^2) comes out superior to any of the individual models in the simulation of the Southern Hemisphere ice extents, followed closely by the ECHAM5 and CSIRO Mk3 models (RMS = 1.6×10^6 km^2). In the simulation of the Northern Hemisphere ice extents, the CGCM3 comes out on top (with an RMS of 0.6×10^6 km^2), followed by the 11-model composite (RMS = 0.7×10^6 km^2) and the MIROC3 and ECHAM5 models (RMS = 0.8×10^6 km^2). Other measures of performance, such as aspects of the spatial distributions, would yield different rankings.

[41] These results essentially show a snapshot of how well the 11 examined GCMs are doing in the simulation of the polar sea ice covers as of the submission of the modeling results for the upcoming IPCC Fourth Assessment Report. All of the models simulate some aspects of the sea ice covers well, but some of the models have severe deficiencies in other aspects, as detailed in section 4 and Figures 2–4. However, model development continues in each of the modeling groups, and hence some of the shortcomings of the model simulations are likely to be improved upon in subsequent versions of the models. By soliciting simulation results from modeling groups from around the world and making them available to interested scientists, the IPCC effort enables comparative studies, such as the one in this paper, that can identify strengths and weaknesses of the results versus the observations and thereby, ideally, can help both in the continuing improvement of the models and in the interpretation of the modeled results.

[42] **Acknowledgments.** The authors greatly appreciate the 11 modeling groups for making their simulation results available and the Program for Climate Model Diagnostics and Intercomparison at Lawrence Livermore National Laboratory for compiling and providing Internet access to these results. We also greatly appreciate Nick DiGirolamo for his help in the processing of the satellite data and in the generation of three of the figures. Andrey Proshutinsky and John Walsh provided thoughtful and much appreciated reviews of the manuscript; *Journal of Geophysical Research* Editors John Klinck and Bruno Tremblay are thanked for their constructive comments and help in moving the manuscript through the review process. This work was supported by the Cryospheric Sciences Program at NASA Headquarters.

References

Aagaard, K., and E. C. Carmack (1989), The role of sea ice and other fresh water in the Arctic circulation, *J. Geophys. Res.*, *94*(C10), 14,485–14,498.

Barry, R. G., M. C. Serreze, J. A. Maslanik, and R. H. Preller (1993), The Arctic sea ice-climate system: Observations and modeling, *Rev. Geophys.*, *31*(4), 397–422.

Cavalieri, D. J., C. L. Parkinson, P. Gloersen, J. C. Comiso, and H. J. Zwally (1999), Deriving long-term time series of sea ice cover from satellite passive-microwave multisensor data sets, *J. Geophys. Res.*, *104*(C7), 15,803–15,814.

Delworth, T. L., et al. (2006), GFDL's CM2 global coupled climate models. part 1: Formulation and simulation characteristics, *J. Clim.*, *19*, 643–674.

Diansky, N. A., and E. M. Volodin (2002), Simulation of present-day climate with a coupled atmosphere-ocean general circulation model, *Izv. Russ. Acad. Sci. Atmos. Oceanic Phys., Engl. Transl.*, *38*(6), 732–747.

Diansky, N. A., A. V. Bagno, and V. B. Zalesny (2002), Sigma model of global ocean circulation and its sensitivity to variations in wind stress, *Izv. Russ. Acad. Sci. Atmos. Oceanic Phys., Engl. Transl.*, *38*(5), 477–494.

Furevik, T., M. Bentsen, H. Drange, I. K. T. Kindem, N. G. Kvamsto, and A. Sorteberg (2003), Description and evaluation of the Bergen climate model: ARPEGE coupled with MICOM, *Clim. Dyn.*, *21*, 27–51.

Gordon, A. L., and H. W. Taylor (1975), Seasonal change of Antarctic sea ice cover, *Science*, *187*, 346–347.

Gordon, C., C. Cooper, C. A. Senior, H. Banks, J. M. Gregory, T. C. Johns, J. F. B. Mitchell, and R. A. Wood (2000), The simulation of SST, sea ice extents and ocean heat transports in a version of the Hadley Centre coupled model without flux adjustments, *Clim. Dyn.*, *16*, 147–168.

Gordon, H. B., et al. (2002), The CSIRO Mk3 Climate System Model, *Atmos. Res. Tech. Pap. 60*, 130 pp., CSIRO, Aspendale, Australia. (Available at http://www.dar.csiro.au/publications/gordon_2002a.pdf)

Hasumi, H., and S. Emori (Eds.) (2004), K-1 Coupled GCM (MIROC) Description, *K-1 Tech. Rep. 1*, 34 pp., Cent. for Clim. Syst. Res., Univ. of Tokyo, Tokyo, Japan. (Available at http://www.ccsr.u-tokyo.ac.jp/kyosei/hasumi/MIROC/tech-repo.pdf)

Hortal, A., and A. J. Simmonds (1991), Use of reduced Gaussian grids in spectral models, *Mon. Weather Rev.*, *119*, 1057–1074.

Houghton, J. T., , Y. Ding, D. J. Griggs, M. Noguer, P. J. van der Linden, X. Dai, K. Maskell, and C. A. Johnson (Eds.) (2001), *Climate Change 2001: The Scientific Basis, Contribution of Working Group 1 to the Third Assessment Report of the Intergovernmental Panel on Climate Change*, 881 pp., Cambridge Univ. Press, New York.

Johns, T., et al. (2005), HadGEM1–Model description and analysis of preliminary experiments for the IPCC Fourth Assessment Report, *Tech. Note 55*, 74 pp., Hadley Cent., Exeter, U.K. (Available at http://www.metoffice.com/research/hadleycentre/pubs/HCTN/HCTN_55.pdf)

Kim, S.-J., G. M. Flato, G. J. Boer, and N. A. McFarlane (2002), A coupled climate model simulation of the Last Glacial Maximum, part 1: Transient multi-decadal response, *Clim. Dyn.*, *19*, 515–537.

Marsland, S. J., H. Haak, J. H. Jungclaus, M. Latif, and F. Röske (2003), The Max-Planck-Institute global ocean/sea ice model with orthogonal curvilinear coordinates, *Ocean Modell.*, *5*, 91–127.

Marti, O., et al. (2005), The new IPSL climate system model: IPSL-CM4, 86 pp., Inst. Pierre Simon Laplace des Sci. de l'Environ. Global, Paris. (Available at http://dods.ipsl.jussieu.fr/omamce/IPSLCM4/Doc-IPSLCM4/FILES/DocIPSLCM4.pdf)

Parkinson, C. L. (2004), Southern Ocean sea ice and its wider linkages: Insights revealed from models and observations, *Antarct. Sci.*, *16*(4), 387–400, doi:10.1017/S0954102004002214.

Parkinson, C. L., D. J. Cavalieri, P. Gloersen, H. J. Zwally, and J. C. Comiso (1999), Arctic sea ice extents, areas, and trends, 1978–1996, *J. Geophys. Res.*, *104*(C9), 20,837–20,856.

Pope, V. D., M. L. Gallani, P. R. Rowntree, and R. A. Stratton (2000), The impact of new physical parameterizations in the Hadley Centre climate model–HadAM3, *Clim. Dyn.*, *16*, 123–146.

Proshutinsky, A., et al. (2001), Multinational effort studies differences among Arctic Ocean models, *Eos Trans. AGU*, *82*(51), 637, 643–644.

Richardson, P. L. (1980), Benjamin Franklin and Timothy Folger's first printed chart of the Gulf Stream, *Science*, *207*(4431), 643–645.

Roeckner, E., et al. (2003), The atmospheric general circulation model ECHAM5, part I, Model description, *Rep. 349*, 127 pp., Max Planck Inst. for Meteorol., Hamburg, Germany.

Russell, G. L., J. R. Miller, D. Rind, R. A. Ruedy, G. A. Schmidt, and S. Sheth (2000), Comparison of model and observed regional temperature changes during the past 40 years, *J. Geophys. Res.*, *105*, 14,891–14,898.

Santer, B. D., et al. (2005), Amplification of surface temperature trends and variability in the tropical atmosphere, *Science*, *309*, 1551–1556. (Supporting material available at www.sciencemag.org/cgi/content/full/1114867/DC1)

Schmidt, G. A., et al. (2006), Present-day atmospheric simulations using GISS ModelE: Comparison to in situ, satellite, and reanalysis data, *J. Clim.*, *19*, 153–192.

Serreze, M. C., J. E. Walsh, F. S. Chapin III, T. Osterkamp, M. Dyurgerov, V. Romanovsky, W. C. Oechel, J. Morison, T. Zhang, and R. G. Barry (2000), Observational evidence of recent change in the northern high-latitude environment, *Clim. Change*, *46*(2), 159–207.

Vinnikov, K. Y., D. J. Cavalieri, and C. L. Parkinson (2006), A model assessment of satellite observed trends in polar sea ice extents, *Geophys. Res. Lett.*, *33*, L05704, doi:10.1029/2005GL025282.

Walsh, J. E., V. M. Kattsov, W. L. Chapman, V. Govorkova, and T. Pavlova (2002), Comparison of Arctic climate simulations by uncoupled and coupled global models, *J. Clim.*, *15*, 1429–1446.

Zhang, R., and T. L. Delworth (2005), Simulated tropical response to a substantial weakening of the Atlantic thermohaline circulation, *J. Clim.*, *18*, 1853–1860.

Zwally, H. J., J. C. Comiso, C. L. Parkinson, D. J. Cavalieri, and P. Gloersen (2002), Variability of Antarctic sea ice 1979–1998, *J. Geophys. Res.*, *107*(C5), 3041, doi:10.1029/2000JC000733.

D. J. Cavalieri and C. L. Parkinson, Cryospheric Sciences Branch, Code 614.1, NASA Goddard Space Flight Center, Greenbelt, MD 20771, USA. (claire.l.parkinson@nasa.gov)

K. Y. Vinnikov, Department of Meteorology, University of Maryland, College Park, MD 20742, USA.